IEEE Access
Multidisciplinary | Rapid Review | Open Access Journal

Received February 3, 2018, accepted March 25, 2018, date of publication April 2, 2018, date of current version April 23, 2018.

Digital Object Identifier 10.1109/ACCESS.2018.2821761

Multi-Slot Coverage Probability and SINR-Based Handover Rate Analysis for Mobile User in Hetnet

XUEFEI ZHANG, (Member, IEEE), YUXUAN XIE, YUSHAN CUI, QIMEI CUI, (Member, IEEE), AND XIAOFENG TAO, (Senior Member, IEEE)

[1]National Engineering Lab for Mobile Network Technologies, Beijing 100876, China
[2]Beijing University of Posts and Telecommunications, Beijing 100876, China

Corresponding author: Xuefei Zhang (zhangxuefei@bupt.edu.cn)

This work was supported in part by the National Nature Science Foundation of China under Grant 61701037, Grant 61471058, and Grant 61631005, in part by the Beijing Natural Science Foundation under Grant L172033, in part by the Beijing Science and Technology Commission Foundation under Grant 201702005, and in part by the 111 Project of China B16006.

ABSTRACT User mobility brings about the spatial correlation in user association (or handover) over a period of multi slots. The correlation makes the classic user association methodology, i.e., typical user method in stochastic geometry, invalid. In addition, the impact of signal to interference plus noise ratio (SINR) on handover cannot be overlooked due to the strong interference caused by the dense base station deployment. To address the above issues, we aim to explore a methodology to analyze the multi-slot network performance for a mobile user considering the SINR effect at the user's location before it moves and the user's location after it moves. The main idea is to find the correlated association (and interference) regions in different time slots. On this basis, the expression of multi-slot coverage probability, SINR-based horizontal, and vertical handover rate are derived under maximum average received power (MARP) strategy. Simulation results prove the positive correlation in the associated distance as well as the multi-slot coverage probability, and the impact of SINR on horizontal and vertical handover rate over a period of multi slots. Moreover, MARP strategy always outperforms the nearest distance strategy on multi-slot coverage probability at the almost same cost of handovers. Finally, we found that increasing the picocell density, transmission powers, and biasing can lead substantial loads offloading to picocell but make no significant contribution to the overall coverage.

INDEX TERMS Multi-slot correlation, SINR-based handover rate, User mobility, Stochastic geometry.

I. INTRODUCTION

Data rates of wireless communications have increased dramatically to 4.2 billion Gbit during the last decade and tend to continue rising exponentially in the next one. To meet the capacity requirement, more heterogeneous lower-power access points have been introduced in wireless cellular networks, i.e. heterogeneous networks (HetNets) [1]. On one hand, HetNets can provide a more flexible and economical network deployment, contributing to the wider coverage and higher data rate [2]; on the other hand, dense deployment of access points leads to the frequent handovers between horizontal or vertical cells, resulting in new impediments to network access [3].

Compared with horizontal handovers, i.e., handovers made between two BSs in the same tier, vertical handovers impact both the MUs and the overall system in more complicated ways. Vertical handover means that handovers happen between two BSs in different tiers. Additional risks, e.g., extra latency and signaling, are present under vertical handover. Furthermore, vertical handovers facing different radio access technologies (e.g., LTE access and WiFi access) could cause performance degradation [4]. Therefore, handover rate, i.e., the number of handovers at a unit time, is a significant metric for HetNets, which must be addressed in an efficient manner to minimize the service delay and connection failure for MUs [5].

Currently, there is a large body of literatures on handover performance analysis. Two main ideas are adopted to analyze the network performance of the case that user is mobile. The first is to follow typical user method in stochastic geometry, which has been proved to be an effective approach to analyze network performance in the random network. This method, together with random geometric graphs, have contributed to some results on the coverage probability, average achievable

rate and other fundamental limits of wireless networks. A tutorial article [6] surveys some of these techniques, discusses their application in wireless networks, and presents some of the main results. Further, typical user method is extended into the performance analysis of HetNet due to the independence of intra- and inter-tier BSs. The closed-form expressions of the coverage probability and the achievable rate using ND, MARP and maximum SINR strategies are derived [7]–[9]. In addition, some focus on the modified network models, e.g., Poisson hole process, Poisson cluster process, or other non-uniform random process to construct BS location, the performance metrics of which are derived using some approximation methods [10]–[13]. Nevertheless, typical user method performs well when the user is static, whereas it turns to invalidity for MU analysis. The reason is that user mobility brings about the correlation of multi-slot associated distances, obeying the independence assumption of typical user method.

The other idea of handover analysis focuses on the cell edge in which handover happens. The handover rate of a MU, i.e., the number of the intersections of MU trajectory and cell edge in a unit time, is analyzed as Buffon's needle problem in [14] and [15], where BS serving zones are modeled as Poisson Voronoi tessellations (PVT). In addition, cell edges are modeled as a fiber process and the handover rate are derived by mapping the 1-D intersection problem into limit of 2-D area intensity in [16]–[18]. However, most of the results are location-dependent regardless of SINR constraint [3]. In [19], the effect of SINR at the user's location before it moves is introduced into the coverage probability analysis. However, the effect of SINR at the user's location after it moves is not considered. In addition, the method in [19] are not applicable to vertical handover rate or coverage probability with vertical handover.

In this paper, we fill in an important gap left by previous work on the performance analysis considering the spatial correlation and SINR effects at the user's location before it moves and the user's location after it moves. Specifically, we aim to explore a methodology to analyze the multi-slot network performance for a mobile user (MU). The main idea is to find the correlated association (and interference) regions in different time slot. Additionally, we incorporate the impact of SINR on the handover rate. On this basis, the pdf of the associated distance, the multi-slot coverage probability, SINR-based horizontal and vertical handover rate are derived. This proposed methodology can also be regarded as a byproduct to analyze the multi-user scenario. Simulation results prove the positive correlation in the associated distance as well as the multi-slot coverage probability, and the impact of SINR on horizontal and vertical handover rate over a period of multi slots. Moreover, MARP strategy always outperforms nearest distance (ND) strategy on multi-slot coverage probability at the almost same cost of handovers. Finally, we found that increasing the picocell density, transmission power and biasing can lead substantial loads offloading to picocell but make no significant contribution to the overall coverage.

In addition to this introductory section, we organized our paper as follows. In Section II, we describe the system model and introduce the performance metrics that will be used in this paper. Next, the pdf of the multi-slot associated distances, multi-slot coverage probability, SINR-based horizontal and vertical handover rate are derived under MARP strategy in Section III. Section IV provided our simulation results and discussion. Finally, we conclude our paper in Section V.

II. SYSTEM MODEL

We consider a HetNet with spatially randomly distributed K tiers of BSs and assume that each tier of BSs independently form a homogeneous Poisson point process (PPP) in two-dimensional Euclidean space $\mathbb{R}^2$. Let λ_k and P_k denote the k-tier BS density and transmission power. A MU moves in a random waypoint (RWP) model during n time slots. A MU movement trace can be formally described by a sequence of triples: $S_i = \{(X_i, d_i, \upsilon_i)\}$ where i denotes the slot index, $i = 1, 2, \ldots, n$. During the i-th slot, X_i denotes the starting waypoint (we assume that X_1 is at origin), d_i denotes the movement distance following a uniform distribution $U(R_{\min}, R_{\max})$, and υ_i denotes the angle of movement direction with respect to the direction of the connection to the associated BS, following a uniform distribution $U(0, 2\pi)$. The movement of a MU in the i-th slot is a Markov process and the starting waypoint X_{i+1} is only decided by the state $S_i = \{(X_i, d_i, \upsilon_i)\}$, i.e., $\Pr(X_i | S_{i-1}, S_{i-2}, \ldots, S_2, S_1) = \Pr(X_i | S_{i-1})$. We use the maximum average received power (MARP) as user association strategy, i.e., MU is associated with the BS with MARP among BSs in all tiers. $R_i(k_i)$ is the associated distance in the i-th slot and implies that the associated BS belongs to k_i tier where k_i is the associated tier in the i-th slot. Therefore, under MARP strategy, no k_i-tier BS exists within the circle centered at X_i with radius $R_i(k_i)$ and no j-tier BS exists within the circle centered at X_i with radius $\eta_i(j)$, where $\eta_i(j) = \sqrt[\alpha]{\frac{P_j}{P_{k_i}}} R_i(k_i)$ is the distance between MU and the nearest j-tier BS in the i-th slot. Notably, j for $\eta_i(j)$ may be different from k_i. If MU associates to the same tier in the first and second slot, $\eta_1(k_2) = R_1(k_1)$ for $k_1 = k_2$.

The SINR of a MU in the i-th slot, denoted by $\gamma(i)$, is given by

$$\gamma(i) = \frac{P_{k_i} h_z(i) |X_i - z|^{-\alpha}}{\sum_{j=1}^{K} \sum_{y \in \Psi_j \setminus z} P_j h_y(i) |X_i - y|^{-\alpha} + \sigma^2} \tag{1}$$

where α is the path loss exponent, $h_z(i)$ is the channel gain from the transmitter at z following Rayleigh fading, Ψ_j is the set of j-tier BSs and σ^2 is the constant additive noise power.

III. MULTI-SLOT PERFORMANCE ANALYSIS

In this section, we explore a new method to analyze multi-slot coverage probability, SINR-based horizontal and vertical handover rate on account of the correlation of multi-slot associated distances. Most of work analyze user association by

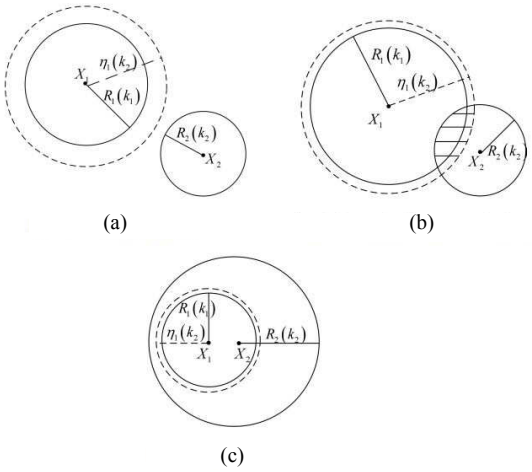

FIGURE 1. Associated distance and interference region in the first two slots under MARP strategy. (a) $d_1 > R_2(k_2) + \eta_1(k_2)$. (b) $|\eta_1(k_2) - R_2(K_2)| \le d_1 > R_2(k_2) + \eta_1(k_2)$. (c) $d_1 < |\eta_1(k_2) - R_2(K_2)|$.

typical user method in stochastic geometry [6]–[10]. Typical user method perform well when the spatial distributions are independent. However, when we consider a MU moving in an arbitrary trajectory, the correlation occurs in two places: one exists in the associated distances over the multi slots; the other occurs at the locations of interference sources in multi slots. These correlations lead to the invalidity of typical user method.

In the following, we first analyze the probability density function (pdf) of associated distance and Laplace transform of aggregated interference by stochastic geometry, but not by typical user method. On this basis, we derive the multi-slot coverage probability, SINR-based horizontal and vertical handover rate.

A. THE PDF OF THE MULTI-SLOT ASSOCIATED DISTANCES

The pdf of the associated distance in the first slot is given by [13]

$$g_{R_1}(r_1(k_1)) = \frac{\partial\left[1 - \Pr\left(R_1\left(k_1\right) > r_1\left(k_1\right)\right)\right]}{\partial r_1\left(k_1\right)} = 2\pi\lambda_{k_1} r_1(k_1) \exp\left(-\pi \sum_{j=1}^{K} \lambda_j \left(\frac{P_j}{P_{k_1}}\right)^{\frac{2}{\alpha}} r_1(k_1)^2\right) \tag{2}$$

and it degenerates to the pdf of the distance between MU and the nearest BS for a single-tier network, denoted by $f_{R_1}\left(r_1\left(k_1\right)\right)$ [3]. The joint pdf of $R_2\left(k_2\right)$ and $R_1\left(k_1\right)$ is

$$g_{R_1R_2}\left(r_1\left(k_1\right), r_2\left(k_2\right)\right) = \frac{\partial \Pr\left(R_1\left(k_1\right) \le r_1\left(k_1\right), R_2\left(k_2\right) \le r_2\left(k_2\right)\right)}{\partial r_1\left(k_1\right) \partial r_2\left(k_2\right)} \tag{3}$$

The joint cumulative distribution function (cdf) is given by (4), as shown at the bottom of this page, where $A_i\left(k_i\right)$ is the area of the circle centered at X_i with radius $R_i\left(k_i\right)$ and $C_l\left(k_j\right)$ is the area of the circle centered at X_l with radius $\eta_l\left(k_j\right)$. $A_i\left(k_i\right) \setminus C_l\left(k_j\right)$ represents the relative complement area of $C_l\left(k_j\right)$ in $A_i\left(k_i\right)$. Using geometry method, $A_2\left(k_2\right) \setminus C_1\left(k_2\right)$ is decided by the value of d_1, $|\eta_1\left(k_2\right) - R_2\left(k_2\right)|$ and $|\eta_1\left(k_2\right) + R_2\left(k_2\right)|$ as is shown in Fig.1 (The proof of $A_2\left(k_2\right) \setminus C_1\left(k_2\right)$ classification is provided in *Appendix A*). $f_{R_1R_2}\left(R_1\left(k_1\right), R_2\left(k_2\right)\right)$, the joint pdf of the distance from MU to the nearest k_1-th tier BS in the first slot and the distance from MU to the nearest k_2-th tier BS in the second slot, is given by

$$f_{R_1R_2}\left(r_1\left(k_1\right), r_2\left(k_2\right)\right) = f_{R_2|R_1}\left(r_2\left(k_2\right)|r_1\left(k_1\right)\right) f_R\left(r_1\left(k_1\right)\right) \tag{5}$$

The associated distance in the second slot $R_2\left(k_2\right)$ is dependent on $R_1\left(k_1\right)$ due to the fact that MU is moving while all BSs are fixed. Therefore, the conditional pdf of $R_2\left(k_2\right)$ conditioned on $R_1\left(k_1\right)$ is

$$\begin{aligned} &f_{R_2|R_1}\left(r_2\left(k_2\right)|r_1\left(k_1\right)\right) \\ &= \frac{\partial\left[1 - \exp\left(-\lambda_k\left(A_2\left(k_2\right) \setminus C_1\left(k_2\right)\right)\right)\right]}{\partial r_2\left(k_2\right)} \\ &= \lambda_{k_2} \exp\left(-\lambda_{k_2}\left(A_2\left(k_2\right) \setminus C_1\left(k_2\right)\right)\right) \frac{\partial\left(A_2\left(k_2\right) \setminus C_1\left(k_2\right)\right)}{\partial r_2\left(k_2\right)} \end{aligned} \tag{6}$$

The area $A_2\left(k_2\right) \setminus C_1\left(k_2\right)$ is expressed as (7) and (8), shown at the top of the next page. According to (3)-(8), we can calculate $g_{R_1R_2}\left(r_1\left(k_1\right), r_2\left(k_2\right)\right)$.

B. THE MULTI-SLOT COVERAGE PROBABILITY

The multi-slot coverage probability is defined as the probability that MU is in the coverage of BSs during all slots, which can be expressed as $\Pr\left(\bigcap_{i=1}^{T} \gamma\left(i\right) \ge \gamma_T\right)$ where γ_T

$$\begin{aligned} &\Pr\left(R_1\left(k_1\right) \le r_1\left(k_1\right), R_2\left(k_2\right) \le r_2\left(k_2\right)\right) \\ &= \Pr\left(R_1\left(k_1\right) \le r_1\left(k_1\right), R_2\left(k_2\right) \le r_2\left(k_2\right), \bigcap_{i=1, i\ne k_1}^{K} R_1\left(k_1\right) < R_1\left(i\right), \bigcap_{j=1, i\ne k_2}^{K} R_2\left(k_2\right) < R_2\left(j\right)\right) \\ &= \int_0^{r_1(k_1)} \int_0^{r_2(k_2)} \prod_{i=1, i\ne k_1}^{K} \exp\left(-\lambda_i A_1\left(k_1\right)\right) \prod_{j=1, j\ne k_2}^{K} \exp\left(-\lambda_j A_2\left(k_2\right) \setminus C_1\left(k_2\right)\right) f_{R_1R_2}\left(R_1\left(k_1\right), R_2\left(k_2\right)\right) dR_1\left(k_1\right) dR_2\left(k_2\right) \end{aligned} \tag{4}$$

$$A_2(k_2)\setminus C_1(k_2)=\begin{cases}\pi r_2(k_2)^2 & d_1\geq \eta_1(k_2)+r_2(k_2)\\ \pi r_2(k_2)^2-\begin{bmatrix}a_1(k_2)\,\eta_1(k_2)^2+a_2(k_2)\,r_2(k_2)^2\\ -\eta_1(k_2)\,d_1\sin(a_1)\end{bmatrix} & |r_2(k_2)-\eta_1(k_2)|<d_1<\eta_1(k_2)+r_2(k_2)\\ \pi r_2(k_2)^2-\pi\eta_1(k_2)^2 & 0<d_1<r_2(k_2)-\eta_1(k_2)\end{cases} \tag{7}$$

where $a_1(j)=acos\left(\frac{\eta_1(j)^2+d_1^2-r_2(j)^2}{2d_1\eta_1(j)}\right)$ and $a_2(j)=acos\left(\frac{r_2(j)^2+d_1^2-\eta_1(j)^2}{2d_1r_2(j)}\right)$ using the law of cosines.

$$\frac{\partial\left(A_2(k_2)\setminus C_1(k_2)\right)}{\partial r_2(k_2)}=\begin{cases}2\pi r_2(k_2) & d_1\geq \eta_1(k_2)+r_2(k_2)\\ [-\eta_1(k_2)^2\frac{\partial a_1(k_2)}{\partial r_2(k_2)}+(\pi-a_2(k_2))\,2r_2(k_2)- & r_2(k_2)-\eta_1(k_2)<d_1<\eta_1(k_2)+r_2(k_2)\\ r_2(k_2)^2\frac{\partial a_2(k_2)}{\partial r_2(k_2)}+\eta_1(k_2)\,d_1\cos(a_1(k_2))\frac{\partial a_1(k_2)}{\partial r_2(k_2)}] & 0<d_1<r_2(k_2)-\eta_1(k_2)\\ 2\pi r_2(k_2)\end{cases} \tag{8}$$

$$\begin{aligned}&\Pr\left(\gamma(1)\geq\gamma_T,\gamma(2)\geq\gamma_T,H_0(1)\,|d_1,r_1(k_1),\upsilon_1\right)\\&=\Pr\left(h_y(1)>\frac{\gamma_T r_1(k_1)^\alpha}{P_{k_1}}\left[\sum_{j=1}^{K}\sum_{z\in\Phi(j)}I_j^1(z)+\sigma^2\right],h_y(2)>\frac{\gamma_T r_2(k_2)^\alpha}{P_{k_2}}\left[\sum_{j=1}^{K}\sum_{z\in\Phi(j)}I_j^2(z)+\sigma^2\right],H_0(1)\right)\\&=\exp\left(-a\sigma^2-b\sigma^2\right)\prod_{j=1}^{K}\left\{\exp\left(-\lambda_j\left(C_2(j)\setminus C_1(j)\right)\right)\left[\exp\left(\sum_{z\in\overline{C_1(j)\bigcup C_2(j)}}\left(-aI_j^1(z)-bI_j^2(z)\right)\right)\right]\right\}\end{aligned} \tag{12}$$

is the SINR threshold. The two-slot coverage probability is given by

$$\begin{aligned}&\Pr\left(\gamma(1)\geq\gamma_T,\gamma(2)\geq\gamma_T\right)\\&=\int_0^{2\pi}\int_{D_{\min}}^{D_{\max}}\Pr\left(\gamma(1)\geq\gamma_T,\gamma(2)\geq\gamma_T\,|d_1,\upsilon_1\right)\\&\quad\cdot\zeta(d_1,\upsilon_1)\,d(d_1)\,d\upsilon_1\end{aligned} \tag{9}$$

where the pdf $\zeta(d_1,\upsilon_1)=\frac{1}{2\pi(R_{\max}-R_{\min})}$ as described in Section II and $\Pr\left(\gamma(1)\geq\gamma_T,\gamma(2)\geq\gamma_T\,|d_1,\upsilon_1\right)$ is calculated as follow,

$$\begin{aligned}&\Pr\left(\gamma(1)\geq\gamma_T,\gamma(2)\geq\gamma_T\,|d_1,\upsilon_1\right)\\&=\sum_{k_1=1}^{K}\int_0^{\infty}\Pr\left(\gamma(1)\geq\gamma_T,\gamma(2)\geq\gamma_T\,|d_1,r_1(k_1),\upsilon_1\right)\\&\quad\cdot g_{R_1}(r_1(k_1))\,dr_1(k_1)\end{aligned} \tag{10}$$

$\Pr\left(\gamma(1)\geq\gamma_T,\gamma(2)\geq\gamma_T\,|d_1,r_1(k_1),\upsilon_1\right)$, including three conditions, i.e., coverage probability under no handover, horizontal handover and vertical handover, is given by

$$\begin{aligned}&\Pr\left(\gamma(1)\geq\gamma_T,\gamma(2)\geq\gamma_T\,|d_1,r_1(k_1),\upsilon_1\right)\\&=\Pr\left(\gamma(1)\geq\gamma_T,\gamma(2)\geq\gamma_T,H_0(1)\,|d_1,r_1(k_1),\upsilon_1\right)\\&\quad+\Pr\left(\gamma(1)\geq\gamma_T,\gamma(2)\geq\gamma_T,H_h(1)\,|d_1,r_1(k_1),\upsilon_1\right)\\&\quad+\Pr\left(\gamma(1)\geq\gamma_T,\gamma(2)\geq\gamma_T,H_v(1)\,|d_1,r_1(k_1),\upsilon_1\right)\end{aligned} \tag{11}$$

where $H_s(i)$ is the handover state between the i-th and the $(i+1)$-th slot and $s\in\{0,h,v\}$ represents no handover, horizontal handover and vertical handover, respectively. Now, we focus on deriving $\Pr(\gamma(1)\geq\gamma_T,\gamma(2)\geq\gamma_T,H_i(1)\,|d_1,r_1(k_1),\upsilon_1)$.

1) THE COVERAGE PROBABILITY OF NO HANDOVER

The coverage probability of no handover is denoted by (12), as shown at the top of this page, where $a=\frac{\gamma_T r_1(k_1)^\alpha}{P_{k_1}}$, $b=\frac{\gamma_T r_2(k_2)^\alpha}{P_{k_2}}$, $r_2(k_2)=\sqrt{r_1^2(k_1)+d_1^2-2r_1(k_1)\,d_1\cos\upsilon_1}$ and $I_j^i(z)$ is the interference from j-tier BS at z in the i-th slot. Referring to (7), we can calculate $C_2(j)\setminus C_1(j)$. $E\left[\exp\left(\sum_{z\in\overline{C_1(j)\bigcup C_2(j)}}\left(-aI_j^1(z)-bI_j^2(z)\right)\right)\right]$ is the aggregated interference averaged over the channel gain. The analysis of the aggregated interference is presented in *Appendix B*.

Then, we substitute (7) and (25) in *Appendix B* into (12) to obtain the coverage probability of no handover $\Pr\left(\gamma(1)\geq\gamma_T,\gamma(2)\geq\gamma_T,H_0(1)\,|d_1,r_1(k_1),\upsilon_1\right)$.

2) THE COVERAGE PROBABILITY OF HORIZONTAL HANDOVER

$$\begin{aligned}&\Pr\left(\gamma(1)\geq\gamma_T,\gamma(2)\geq\gamma_T,H_h(1)\,|d_1,r_1(k_1),\upsilon_1\right)\\&=\Pr\left(\gamma(1)\geq\gamma_T,\gamma(2)\geq\gamma_T,H_h(1)\,|d_1,r_1(k_1)\right)\end{aligned}$$

$$= \int_0^{\eta_1(k_2)+d_1} \Pr\left(\gamma\left(1\right) \geq \gamma_T, \gamma\left(2\right) \geq \gamma_T, H_h(1) \left| d_1 \right.,\right.$$
$$\left. r_1\left(k_1\right), r_2\left(k_2\right)\right) g\left(r_2\left(k_1\right) \left| r_1\left(k_1\right)\right.\right) dr_2\left(k_1\right) \quad (13)$$

where $\Pr(\gamma\left(1\right) \geq \gamma_T, \gamma\left(2\right) \geq \gamma_T, H_h\left(1\right) | d_1, r_1\left(k_1\right), r_2\left(k_2\right))$ is the coverage probability of the horizontal handover between the first and second slot conditioned on the associated distances $r_1\left(k_1\right)$ and $r_2\left(k_2\right)$ for $k_1 = k_2 = k$.

$$\Pr\left(\gamma\left(1\right) \geq \gamma_T, \gamma\left(2\right) \geq \gamma_T, H_h\left(1\right) | d_1, r_1\left(k\right), r_2\left(k\right)\right)$$
$$= \exp\left(-(a+b)\sigma^2\right) \cdot \prod_{j=1}^{K} E\left[\exp\left(\sum_{z\in\Phi(j)}\left(-aI_j^1\left(z\right) - bI_j^2\left(z\right)\right)\right)\right] \quad (14)$$

where $\Phi\left(j\right)$ is the set of interference BSs in the j-th tier.

(1) If $j \neq k$, $E\left[\exp\left(\sum_{z\in\Phi(j)}\left(-aI_j^1\left(z\right) - bI_j^2\left(z\right)\right)\right)\right]$ is given by (25) in *Appendix B*.

(2) If $j = k$

$$E\left[\exp\left(\sum_{z\in\Phi(j)}\left(-aI_j^1\left(z\right) - bI_j^2\left(z\right)\right)\right)\right]$$
$$= E_{z'}\left[\frac{1}{1+bP_j|X_2 - z'|^{-\alpha}}\right] E_{z''}\left[\frac{1}{1+aP_j|X_1 - z''|^{-\alpha}}\right]$$
$$\times \exp\left\{-\lambda_j \int_{z\in\overline{C_1(j)\bigcup C_2(j)}} F_1\left(l_1, \theta_1\right) dz\right\} \quad (15)$$

where z' is the location of the associated BS in the first slot and z'' is the location of the associated BS in the second slot. The first term in (15) represents the effect of interference caused by the first-slot associated BS to MU in the second slot,

$$E_{z'}\left[\frac{1}{1+bP_j|X_2 - z'|^{-\alpha}}\right] = \frac{1}{(\pi - a_1\left(k\right))}$$
$$\times \int_{a_1(k)}^{\pi} \frac{1}{1+bP_k\sqrt{r_1(k)^2 + d_1^2 - 2r_1\left(k\right)d_1\cos\upsilon_1}^{-\alpha}} d\upsilon_1 \quad (16)$$

where $a_1\left(k\right)$ has been derived below (7), τ_1 is the angle of movement direction with respect to the direction of MU connecting to the first-slot associated BS, the candidate locations of the first-slot associated BS constitute the red arc in Fig.2. The second term in (15) represents the effect of interference caused by the second-slot associated BS to MU in the first slot

$$E_{z''}\left[\frac{1}{1+aP_j|X_1 - z''|^{-\alpha}}\right] = \frac{1}{(\pi - a_2\left(k\right))}$$
$$\times \int_{a_2(k)}^{\pi} \frac{1}{1+aP_k\sqrt{r_2(k)^2 + d_1^2 - 2r_2\left(k\right)d_1\cos\tau_2}^{-\alpha}} d\tau_2 \quad (17)$$

where $a_2\left(k\right)$ has been derived below (7), τ_2 is the angle of movement direction with respect to the direction of

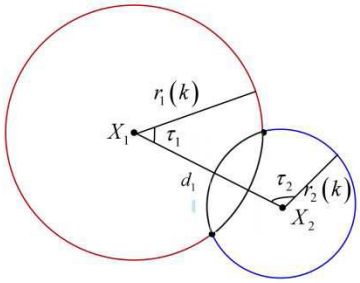

FIGURE 2. The candidate location of the associated BS (red arc is the candidate locations of the first-slot associated BS and blue arc is the candidate locations of the second-slot associated BS).

MU connecting to the second-slot associated BS, the candidate locations of the second-slot associated BS constitute the blue arc in Fig.2. The third term is given by (25) in *Appendix B*. Then, we substitute (14) and $g_{R_1R_2}\left(r_1\left(k_1\right) | r_2\left(k_2\right)\right) = \frac{g_{R_1R_2}(r_1(k_1), r_2(k_2))}{g_{R_1}(r_1(k_1))}$ into (13) to obtain the coverage probability of horizontal handover $\Pr\left(\gamma\left(1\right) \geq \gamma_T, \gamma\left(2\right) \geq \gamma_T, H_h\left(1\right) | d_1, r_1\left(k_1\right), \upsilon_1\right)$.

3) THE COVERAGE PROBABILITY OF VERTICAL HANDOVER

$$\Pr\left(\gamma\left(1\right) \geq \gamma_T, \gamma\left(2\right) \geq \gamma_T, H_v(1) | d_1, r_1\left(k_1\right), \upsilon_1\right)$$
$$= \Pr\left(\gamma\left(1\right) \geq \gamma_T, \gamma\left(2\right) \geq \gamma_T, H_h(1) | d_1, r_1\left(k_1\right)\right)$$
$$= \int_0^{\eta_1(k_2)+d_1} \Pr\left(\gamma\left(1\right) \geq \gamma_T, \gamma\left(2\right) \geq \gamma_T,\ H_v\left(1\right) | d_1\right.,$$
$$\left. r_1\left(k_1\right), r_2\left(k_2\right)\right) g\left(r_2\left(k_1\right) \left| r_1\left(k_1\right)\right.\right) dr_2\left(k_1\right) \quad (18)$$

where $\Pr(\gamma\left(1\right) \geq \gamma_T, \gamma\left(2\right) \geq \gamma_T,\ H_v\left(1\right) | d_1, r_1\left(k_1\right), r_2\left(k_2\right))$ is coverage probability of vertical handover between the first and second slot conditioned on the associated distances $r_1\left(k_1\right)$ and $r_2\left(k_2\right)$,

$$\Pr\left(\gamma\left(1\right) \geq \gamma_T, \gamma\left(2\right) \geq \gamma_T, H_v\left(1\right) | d_1, r_1\left(k_1\right), r_2\left(k_2\right)\right)$$
$$= \exp\left(-a\sigma^2 - b\sigma^2\right) \prod_{j=1}^{K} E\left[\exp\left(\sum_{z\in\Phi(j)}\left(-aI_j^1\left(z\right) - bI_j^2\left(z\right)\right)\right)\right] \quad (19)$$

(1) If $j \neq k_1$ and $j \neq k_2$,

$$E\left[\exp\left(\sum_{z\in\Phi(j)}\left(-aI_j^1\left(z\right) - bI_j^2\left(z\right)\right)\right)\right]$$

is given by (25).

(2) If $j{=}k_1$ and $j \neq k_2$,

$$E\left[\exp\left(\sum_{z\in\Phi(j)}\left(-aI_j^1\left(z\right) - bI_j^2\left(z\right)\right)\right)\right]$$
$$= E_{z'}\left[\frac{1}{1+bP_j|X_2 - z'|^{-\alpha}}\right]$$
$$\times \exp\left\{-\lambda_j \int_{z\in\overline{C_1(j)\bigcup C_2(j)}} F_1\left(l_1, \theta_1\right) dz\right\} \quad (20)$$

where $E_{z'}\left[\frac{1}{1+bP_j|X_2 - z'|^{-\alpha}}\right]$ is given by (16).

(3) If $j{=}k_2$ and $j \neq k_1$,

$$E\left[\exp\left(\sum_{z\in\Phi(j)}\left(-aI_j^1(z)-bI_j^2(z)\right)\right)\right] = E_{z''}\left[\frac{1}{1+aP_j|X_1-z''|^{-\alpha}}\right] \times \exp\left\{-\lambda_j\int_{z\in\overline{C_1(j)\bigcup C_2(j)}}F_1(l_1,\theta_1)dz\right\} \quad (21)$$

where $E_{z''}\left[\frac{1}{1+aP_j|X_1-z''|^{-\alpha}}\right]$ is given by (17).

C. THE SINR-BASED HORIZONTAL AND VERTICAL HANDOVER RATE

The SINR-based handover rate is defined as the probability that a MU successfully connects (satisfying SINR threshold) to two BSs before and after handover, along a moving distance in a unit of time. When moving distance is small, it is reasonable to assume that the handover happens only one time or does not happen. In the following, we derive SINR-based horizontal and vertical handover rate, respectively.

The SINR-based horizontal handover rate can be expressed as

$$E[H_h] = \Pr(\gamma(1)\geq\gamma_T, \gamma(2)\geq\gamma_T,\ H_h(1)) = \sum_{k=1}^{K}\int_{D_{\min}}^{D_{\max}}\int_0^{\infty}\Pr(\gamma(1)\geq\gamma_T,\gamma(2)\geq\gamma_T,\ H_h(1)\,|d_1,\ r_1(k),v_1)\,g_{R_1}(r_1(k))\,\zeta(d_1,v_1)\,dr_1(k)\,d(d_1)\,d(v_1) \quad (22)$$

where $\Pr(\gamma(1)\geq\gamma_T,\gamma(2)\geq\gamma_T,H_h(1)\,|d_1,r_1(k_1),\upsilon_1)$ and $g_{R_1}(r_1(k))$ are given by (13) and (2).

The SINR-based vertical handover rate can be calculated by

$$E[H_v] = \Pr(\gamma(1)\geq\gamma_T,\gamma(2)\geq\gamma_T,\ H_v(1)) = \sum_{k_1=1}^{K}\sum_{k_2=1,k_2\neq k_1}^{K}\int_0^{\infty}\int_0^{\eta_1(k_2)+d_1}\Pr(\gamma(1)\geq\gamma_T,\gamma(2)\geq\gamma_T, H_v(1)\,|d_1,r_1(k_1),r_2(k_2))\,g_{R_1R_2}(r_1(k_1),r_2(k_2)) \times\zeta(d_1)\,dr_2(k_2)\,dr_1(k_1)\,d(d_1) \quad (23)$$

where $\Pr(\gamma(1)\geq\gamma_T,\gamma(2)\geq\gamma_T,H_v(1)\,|d_1,r_1(k_1),r_2(k_2))$ and $g_{R_1R_2}(r_1(k_1),r_2(k_2))$ are given by (19) and (3).

Corollary 1: For a single-tier ($K=1$, we omit the tier index) random network, if it is interference-free and noise-free, i.e., $\sigma^2=0$ and $\gamma_T=0$, no handover probability conditioned on moving distance d_1 can be expressed as

$$\Pr(H_0(1)\,|d_1) = \int_0^{2\pi}\int_0^{\infty}\lambda r_1\exp\left(-\lambda\left(A_1\bigcup A_2\right)\right)dr_1d\upsilon_1 \quad (24)$$

where $A_1\bigcup A_2 = r_1^2(\pi-\upsilon_1+\sin\upsilon_1\cos\upsilon_1)+r_2^2(\pi-\upsilon_2+\sin\upsilon_2\cos\upsilon_2)$, $r_2^2 = r_1^2+d_1^2-2r_1d_1\cos\upsilon_1$ and $\upsilon_2 = arcos\left(\frac{r_2^2+d_1^2-r_1^2}{2r_2d_1}\right)$. This result consists with the result in [31]. The handover rate condition on distance d_1 can be calculated by $\Pr(H_h((1)\,|d_1)=1-\Pr(H_0(1)\,|d_1)$.

Remark 1: The proposed methodology above transforms the correlation in time domain into space domain (e.g., the correlated distance and correlated interference region). Therefore, a n-user scenario involving space-domain correlation can utilized the proposed methodology directly, i.e., a n-user scenario can be considered as a n-slot scenario.

IV. SIMULATION RESULTS

In this section, we present simulation results to evaluate the network performance considering the user mobility. The scenario is a two-tier heterogeneous network, where BSs are located randomly as two independent PPP in a 10km*10km square. MU trajectory is randomly generated, following the mobility described in Section II. Each data point in the figures is averaged over 20000 simulation rounds. The simulation parameters are listed in Table 1.

TABLE 1. Simulation Parameters.

Parameters	Values
The number of time slots	$n=1,2,5$
The MU mobility model	Random waypoint (RWP) model with $R_{min}=0$, $R_{max}=50m$
Macro and pico BS density	$\lambda_1=10^{-6}/m^2$, $\lambda_2=[1:8]\lambda_1$
Path loss exponent of macrocell and picocell	$\alpha_1=3,4$, $\alpha_2=3,4$
SINR threshold	$\gamma_T=1$
The transmission power of macro and pico BSs	$P_1=46$dBm, $P_2=[22:46]$dBm

Fig.3 shows that the pdf of r_1 is a unimodal function, which is the same to that of the static user [13]. In Fig.4(a), the analytical result on joint pdf of r_1 and r_2 under $r_1+r_2>d$ is a unimodal but truncated function due to the fact that r_2 must be no larger than r_1+d, whose partial enlarged drawings are illustrated in Fig.4(b). The jump point of the conditioned pdf of r_2 given fixed r_1 results from the precision loss of computers under two tangent circle conditions, i.e., $r_1+r_2=d$, $r_1-r_2=d$ and $r_2-r_1=d$. Moreover, Fig.4(b) also indicates that the peak of r_2 moves to larger value with the

$$E\left[\exp\left(\sum_{z\in\overline{C_1(j)\bigcup C_2(j)}}\left(-aI_j^1(z)-bI_j^2(z)\right)\right)\right] = E_{h_z(1)h_z(2)}\left[\prod_{z\in\overline{C_1(j)\bigcup C_2(j)}}\exp\left(-aP_jh_z(1)|X_1-z|^{-\alpha}-bP_jh_z(2)|X_2-z|^{-\alpha}\right)\right] \overset{(a)}{=} \exp\left\{-\lambda_j\int_{z\in\overline{C_1(j)\bigcup C_2(j)}}\left[1-\frac{1}{\left(1+aP_jl_1^{-\alpha}\right)\left(1+bP_jg_2(l_1,\theta_1,d_1)^{-\alpha}\right)}\right]dz\right\} \quad (25)$$

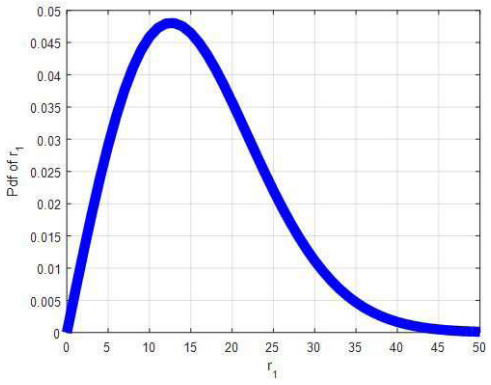

FIGURE 3. Pdf of the associated distance in the first slot .

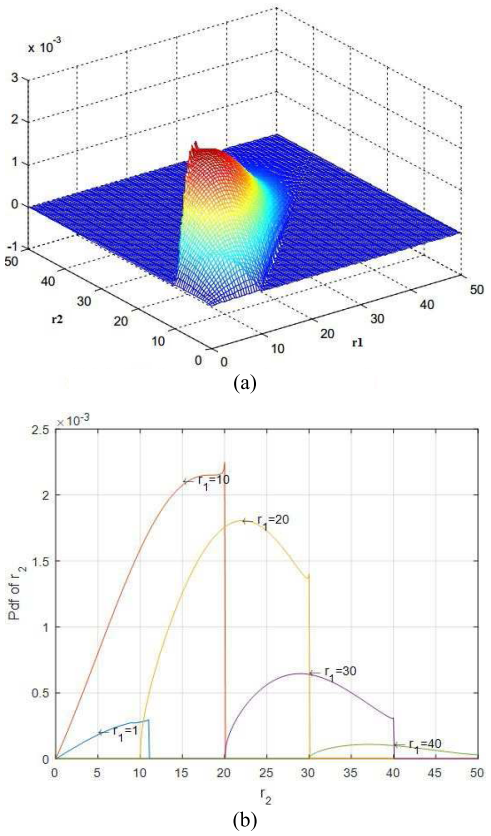

FIGURE 4. Pdf of the associated distance in the first slot .

growth of r_1, which verifies the positive correlation between r_1 and r_2.

In Fig.5, the analytical result on joint pdf of r_1 and r_2 under $r_1 + r_2 < d$ degenerates into the product of two pdf of associated distance in a single slot due to the independence of two far away MU locations.

Fig.6 presents the coverage probability in terms of the ratio of pico BS density to macro BS density under the MARP and ND strategy, respectively. The gaps between the (multi-slot) coverage probabilities over one-slot, two-slot and five-slot scenario, prove that the correlations indeed exist over the multi slots. The multi-slot coverage probability remains almost same with the increasing of $\frac{\lambda_2}{\lambda_1}$ for MARP and that of

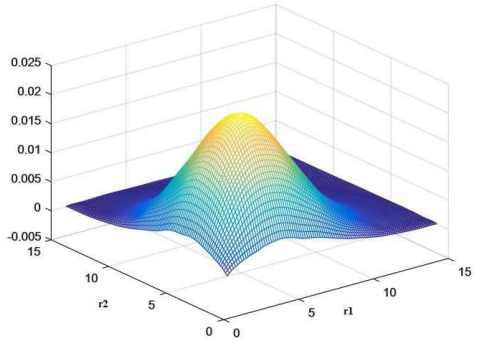

FIGURE 5. Joint pdf of r_1 and r_2 under $r_1 + r_2 < d$.

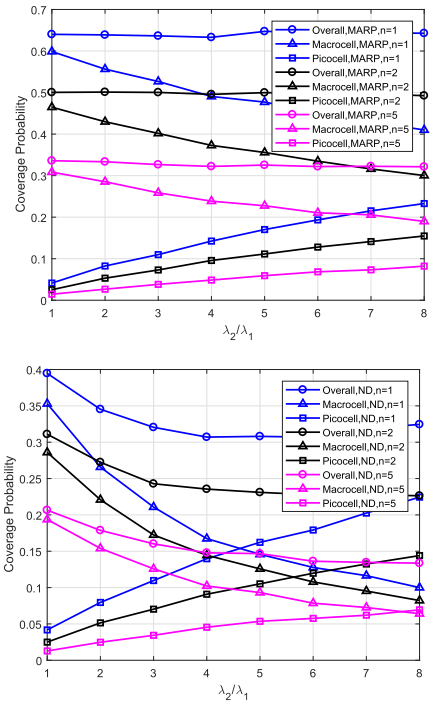

FIGURE 6. Multi-slot coverage probability for the varying $\frac{\lambda_2}{\lambda_1}$.

ND is a slight decrease. That indicates that deploying more BSs is not an effective approach to improve the coverage probability due to the strong interference caused by the high BS deployment density. Although the results of [20] tell us that the throughput is improved with the increasing BS density, it is not the focus of some new emerging small-data service in Internet of Things (IoT). Therefore, simply deploying more BS is not an efficient method to improve the coverage probability for MU. Some interference-free technologies, such as mmWave, can be combined with the more BS deployment method to improve the network coverage. Our previous work [21] proved that mmWave transmission technology adopted in picrocell while the traditional cellular frequencies used in macrocell can significantly improve the coverage probability.

Although the overall coverage probability only has a slight descending with the growth of $\frac{\lambda_2}{\lambda_1}$, it is observed that the

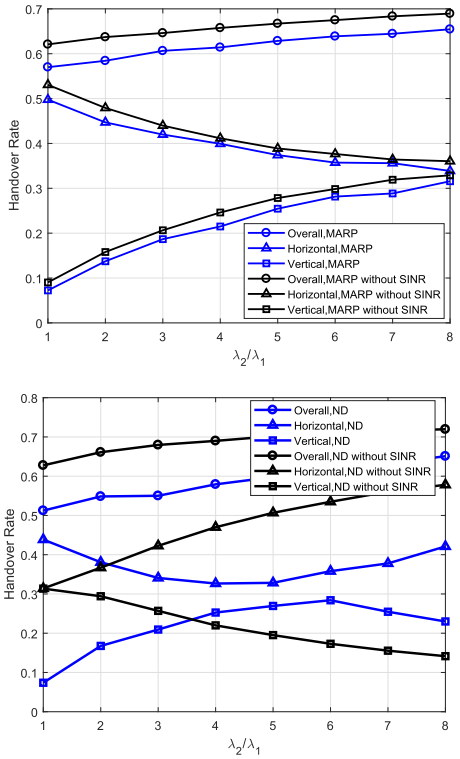

FIGURE 7. Handover rate for the varying $\frac{\lambda_2}{\lambda_1}$.

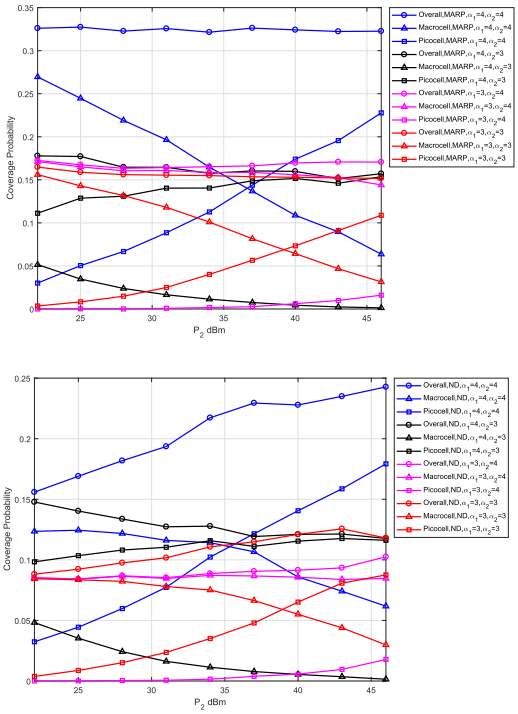

FIGURE 8. Multi-slot coverage probability for varying P_2 .

macrocell coverage decreases at the cost of an increase in picocell for both MARP and ND strategies. As expected, macrocells undertake most of load for $\frac{\lambda_2}{\lambda_1} = 1$ due to the higher transmission power of macrocell.

Similarly, the handover rate is not sensitive to the variation of $\frac{\lambda_2}{\lambda_1}$ as is shown in Fig.7, since the gain from more BS deployment is counterbalanced by the interference that is going on. The gap between the strategy with and without SINR constraint proves the significance of considering the impact of SINR. With the increasing of $\frac{\lambda_2}{\lambda_1}$, MARP has an ascending vertical handover rate and a descending horizontal handover rate while ND gains the opposite results. As we know that vertical handover conducts at higher cost and more complex procedure compared to horizontal handover. Therefore, MARP is potential for low BS deployment and ND is appropriate for high BS deployment. Moreover, we observe that the horizontal handover rate equals to the vertical handover rate for $\frac{\lambda_2}{\lambda_1} = 1$ under ND strategy without considering the impact of SINR. This is because ND strategy is purely position-dominant and positions of BSs following two-tier homogeneous PPP are independent and uniform, which results in the indiscrimination of horizontal and vertical handover.

The plots in Fig.8 show the coverage probability versus the picocell transmission power under different pass loss exponents. The macrocell load decreases at the cost of an increase in picocell load for both MARP and ND strategies. Moreover, macrocell and picocell coverage probability experience substantial changes under $\alpha_1 = \alpha_2$ compared to those under $\alpha_1 \neq \alpha_2$ due to the condition that transmission power is the sole variable under $\alpha_1 = \alpha_2$.

Additionally, the results under large path loss exponents is better than those under small path loss exponents. The reason is that high path loss can isolate the interference that is still the dominant factor in the two-tier scenario considering a typical value of BS density. The exceptional case happens in high macrocell path loss exponent and low picocell path loss exponent, where the overall multi-slot coverage probability of ND strategy experiences a declining along with the picocell transmission power increasing as is shown in Fig.8(b), which proves again that high path loss is capable of isolating the interference.

Agreeing with our intuitions, the horizontal and vertical handover rate without considering the impact of SINR is higher than SINR-based ones in Fig.9. It is observed that the SINR-based horizontal handover rate decreases at low transmission power and increases at high transmission power under MARP strategy, while the SINR-based vertical experience the opposite trend. The symmetric changes for the SINR-based horizontal and vertical handover keep the overall handover rate almost stable. As the results of MARP strategy in Fig.9(a) show, an inflection point appears in both macrocell and picrocell curves with the growth of picrocell transmission power for $\alpha_1 = \alpha_2$ while horizontal/vertical handover rate remains monotonous rising/falling for $\alpha_1 \neq \alpha_2$. Together with the results in Fig.8, we can conclude that macrocell users offloading to picocell causes more vertical handovers at the beginning of P_2 growing then horizontal handovers between picocells play the dominant role when picocell undertakes more loads. In addition, ND strategy without considering

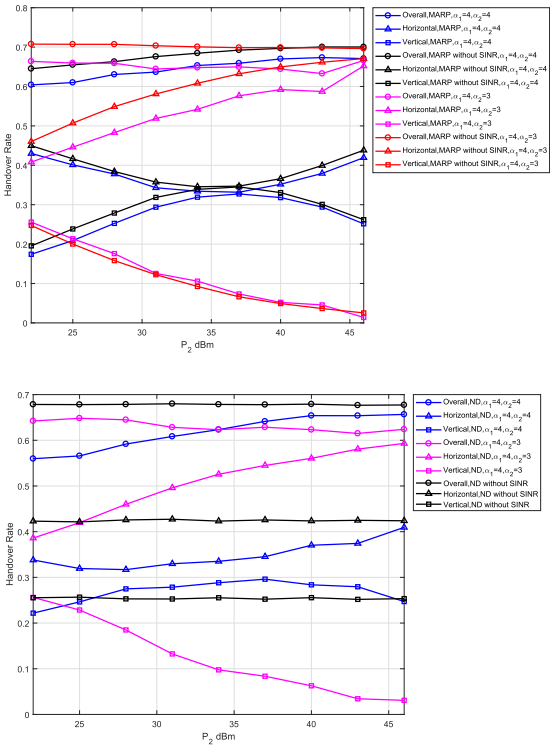

FIGURE 9. Handover rate for varying P_2 .

the impact of SINR is independent of picocell transmission power as is shown in Fig.9(b).

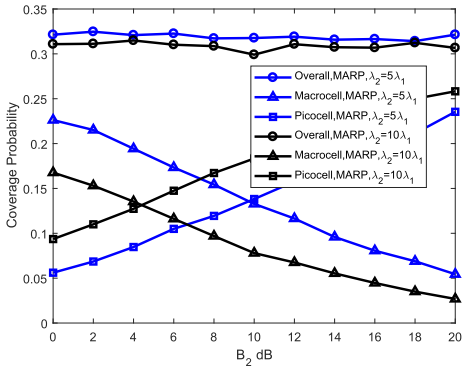

FIGURE 10. Multi-slot coverage probability for varying bias .

ND strategy will not be affected by biasing due to its distance-dominant nature. Therefore, we only explore the effects of biasing under MARP strategy. Fig.10 shows the multi-slot coverage probability in terms of picocell bias factor and BS density for MARP. As the picocell bias factor increases, more MUs are offloaded to the picocell. Intuitively, in biased association, some users are associated with the BS not offering the strongest received signal, which reduces the SINR of the users. But the results in Fig.10 reveal that biasing does not strongly affect the coverage of the overall network under MARP strategy, which is an unexpected but reasonable result due to the fact that the objective of coverage probability is to make SINR satisfy the SINR threshold instead of pursuing the value of SINR as large as possible. Biasing will not result in interference growth so it will cause serious SINR deterioration. In Fig.10, for a given bias factor, deploying more pico BSs decreases the macrocell coverage probability (which means an increase in the picocell coverage), because more MUs are associated with the picocell.

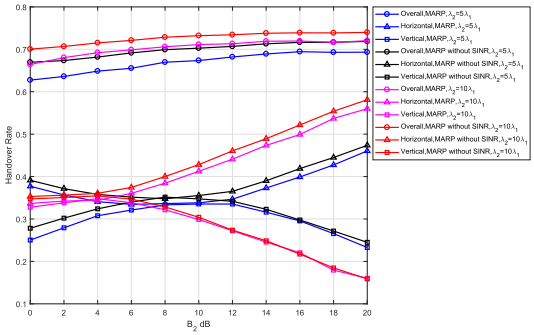

FIGURE 11. Handover rate for varying bias .

Fig.11 shows that the overall handover rate are improved since adding more pico BSs tends to reduce each picocell coverage area. It is intuitively adopted that both the horizontal and the vertical handover rate without considering the impact of SINR are always larger than those considering the impact of SINR. More specifically, the horizontal rate without considering the impact of SINR goes down to a bottom and then rises as biasing enhances continually. The reason is that MUs originally prefer to macrocell for a small bias factor and conduct the vertical handover to the picocell with the increasing of biasing. When the bias factor is large enough, i.e., most of MUs have associated to picocells, the handovers commonly happen between picocells. At this moment, horizontal handover plays a dominant role. The change of vertical handover rate is on the contrary.

Based on the analytical and simulation results, we can conclude that

(1) User mobility indeed brings positive correlation into the associated distances and multi-slot coverage probability.

(2) The gap between SINR-based and SINR-free handover rate indicates the effect of interference on the handover. Specifically, the gap under ND strategy is more obvious than that of MARP strategy. That means that MARP strategy is more robust to the interference.

(3) MARP strategy always outperforms ND strategy on multi-slot coverage probability at the almost same cost of handovers.

(4) Increasing the picocell density, transmission power and biasing can lead substantial loads to picocell but make no significant contribution to the overall coverage. This implies that on one hand it is difficult to achieve substantial coverage improvement only depending on the methods (e.g. denser BS deployment, higher transmission power, etc), which are limited by the interference; on the other hand, these methods are potential to eliminate the macrocell load to picocell.

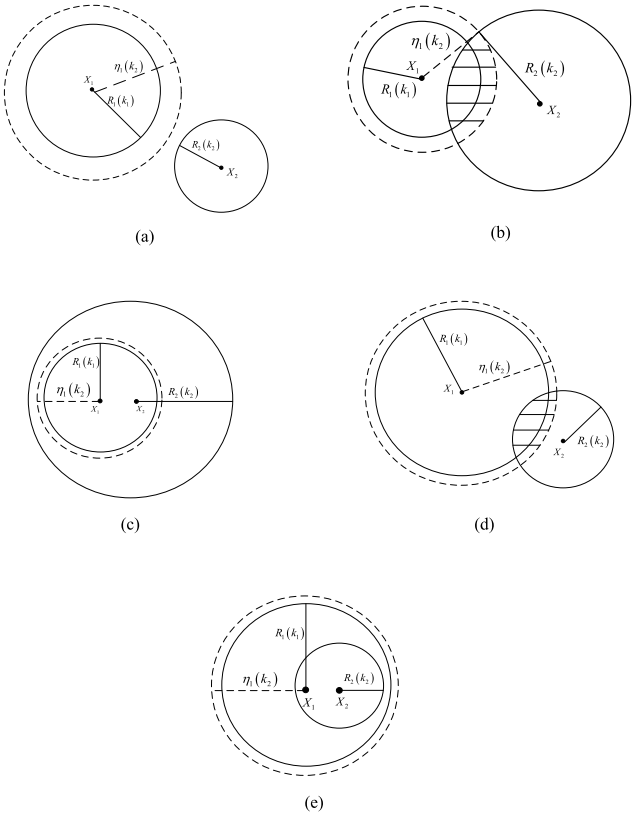

FIGURE 12. Associated distance and interference region in the first two slots. (a) Case 1: $d_1 > R_2(k_2) + \eta_1(k_2)$. (b) Case 2: $R_2(k_2) > \eta_1(k_2)$ and $R_2(k_2) - \eta_1(k_2) \le d_1 \le R_2(k_2) + \eta_1(k_2)$. (c) Case 3: $R_2(k_2) > \eta_1(k_2)$ and $0 < d_1 < R_2(k_2) - \eta_1(k_2)$. (d) Case 4: $R_2(k_2) < \eta_1(k_2)$ and $\eta_1(k_2) - R_2(k_2) \le d_1 \le R_2(k_2) + \eta_1(k_2)$. (e) Case 5: $R_2(k_2) < \eta_1(k_2)$ and $0 < d_1 < \eta_1(k_2) - R_2(k_2)$.

V. CONCLUSION

This paper considers a multi-tier heterogeneous network, considering the spatial correlation caused by user mobility and SINR effect over a period of multi-slots. The expressions of associated distance, multi-slot coverage probability and SINR-based horizontal and vertical handover rate are derived. Simulation results prove that user mobility indeed brings positive correlation into the associated distances in different time slots. Additionally, the gap between the SINR-based and SINR-free handover rate indicates the effect of interference on the handover. Specifically, the gap under ND strategy is more obvious than that of MARP strategy, which means that MARP strategy is more robust to the interference. MARP strategy always outperforms ND strategy on multi-slot coverage probability at the almost same cost of handovers. Finally, increasing the picocell density, transmission power and biasing can lead substantial loads to picocell but make no significant contribution to the overall coverage.

APPENDIX A

Regardless of the specific association strategy, the mathematic relationship between d_1, $R_2(k_2)$ and $\eta_1(k_2)$ have five possible cases as follow Case 1: $d_1 > R_2(k_2) + \eta_1(k_2)$ as is shown in Fig.12(a). Case 2: $R_2(k_2) > \eta_1(k_2)$ and $R_2(k_2) - \eta_1(k_2) \le d_1 \le R_2(k_2) + \eta_1(k_2)$ as is shown in Fig.12(b). Case 3: $R_2(k_2) > \eta_1(k_2)$ and $0 < d_1 < R_2(k_2) - \eta_1(k_2)$ as is shown in Fig.12(c). Case 4: $R_2(k_2) < \eta_1(k_2)$ and $\eta_1(k_2) - R_2(k_2) \le d_1 \le R_2(k_2) + \eta_1(k_2)$ as is shown in Fig.12(d). Case 5: $R_2(k_2) < \eta_1(k_2)$ and $0 < d_1 < \eta_1(k_2) - R_2(k_2)$ as is shown in Fig.12(e).

For the five possible cases, Case 5 will not happen under the maximum average received power (MARP) association strategy owing to the consequence of the first slot that no k_2-tier BS exist within the circle centered at X_1 with radius $\eta_1(k_2)$. Moreover, Case 2 and Case 4 may be integrated into $|R_2(k_2) - \eta_1(k_2)| \le d_1 \le R_2(k_2) + \eta_1(k_2)$. Thus, the relationship between d_1, $R_2(k_2)$ and $\eta_1(k_2)$ are summarized as three classifications, specifically including $d_1 > R_2(k_2) + \eta_1(k_2)$, $|R_2(k_2) - \eta_1(k_2)| \le d_1 \le R_2(k_2) + \eta_1(k_2)$ and $0 < d_1 < R_2(k_2) - \eta_1(k_2)$ for $R_2(k_2) > \eta_1(k_2)$.

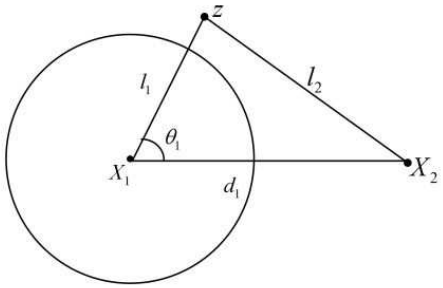

FIGURE 13. Interference from a non-serving BS.

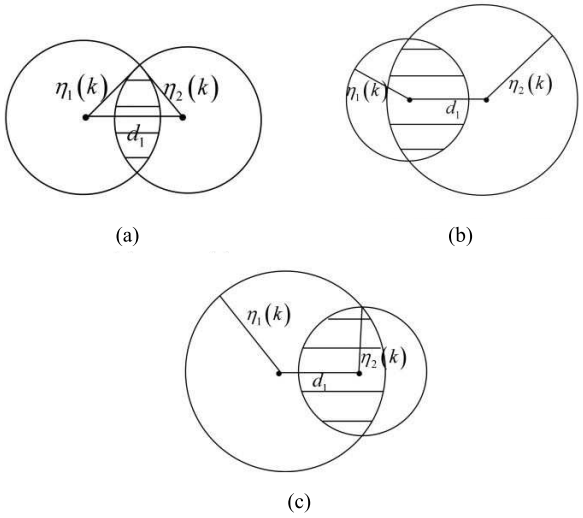

FIGURE 14. Further classification for region $\{C_1(j) \cap C_2(j) \neq \emptyset\} \cap \{C_1(j) \cup C_2(j) \neq C_2(j)\}$.

APPENDIX B

The aggregated interference averaged over the channel gain $E\left[\exp\left(\sum_{z \in \overline{C_1(j) \bigcup C_2(j)}} \left(-aI_j^1(z) - bI_j^2(z)\right)\right)\right]$ is given by

$$\int_{C_1(j)\bigcap C_2(j)} F_1(l_1,\theta_1)dz = \begin{cases} \int_{-a_1(j)}^{a_1(j)}\int_{e_1(j)}^{\eta_1(j)} F_1(l_1,\theta_1)\, l_1 dl_1 d\theta_1 & d_1 > \eta_1(j), \eta_2(j) \\ \left(\int_{-a_1(j)}^{a_1(j)}\int_0^{\eta_1(j)} + \int_{a_1(j)}^{\pi}\int_0^{e_2(j)} + \int_{-\pi}^{-a_1(j)}\int_0^{e_2(j)}\right) F_1(l_1,\theta_1)\, l_1 dl_1 d\theta_1 & \eta_1(j) < d_1 < \eta_2(j) \\ \left(\int_{-a_2(j)}^{a_2(j)}\int_0^{\eta_2(j)} + \int_{a_2(j)}^{\pi}\int_0^{e_2(j)} + \int_{-\pi}^{-a_2(j)}\int_0^{e_2(j)}\right) F_2(l_2,\theta_2)\, l_2 dl_2 d\theta_2 & \eta_2(j) < d_1 < \eta_1(j) \end{cases} \quad (28)$$

(25) where l_i is the distance between X_i and the interference BS at z, θ_i is the angle between MU moving direction in the i-th slot and l_i direction, as is shown in Fig.13. Therefore, l_2 can be uniquely determined by l_1, θ_1 and d_1, denoted by $l_2 = g_2(l_1, \theta_1, d_1)$. Equation (a) in (25) follows from the probability generating functional (PGFL) of PPP. The interference area $\overline{C_1(j)\bigcup C_2(j)} = \overline{C_1(j)} - C_2(j) + C_1(j)\bigcap C_2(j)$, is the algebraic sum of three symmetric shapes. Following are the interference analysis under the three cases, as is shown in Fig.14.

In order for the writing simplification, we define $F_1(l_1,\theta_1) = 1 - \frac{1}{\left(1+aP_j l_1^{-\alpha}\right)\left(1+bP_j g_2(l_1,\theta_1,d_1)^{-\alpha}\right)}$ and $F_2(l_2,\theta_2) = 1 - \frac{1}{\left(1+aP_j g_1(l_2,\theta_2,d_1)^{-\alpha}\right)\left(1+bP_j l_2^{-\alpha}\right)}$. The result of the first integral area is

$$\int_{\overline{C_1(j)}} F_1(l_1,\theta_1)dz = \int_0^{2\pi}\int_{\eta_1(j)}^{\infty} F_1(l_1,\theta_1)\, l_1 dl_1 d\theta_1 \quad (26)$$

The result of the second integral area is

$$\int_{C_2(j)} F_1(l_1,\theta_1)dz = \int_{C_2(j)} F_2(l_2,\theta_2)dz = \int_0^{2\pi}\int_0^{\eta_2(j)} F_2(l_2,\theta_2)\, l_2 dl_2 d\theta_2 \quad (27)$$

The result of the last integral area can be deduced readily for $C_1(j)\bigcap C_2(j)=\emptyset$ (as Fig. 1(a)) and $C_1(j) \subset C_2(j)$ (as Fig. 1(c)), and the remaining condition is further classified, as is given by (28), as shown at the top of this page, where $a_1(j)$ has been derived below (7), $e_1(j) = d_1\cos\alpha_1 - \sqrt{\eta_2(j)^2 - d_1^2\sin^2\alpha_1}$ and $e_2(j) = d_1\cos\alpha_1 + \sqrt{\eta_2(j)^2 - d_1^2\sin^2\alpha_1}$.

REFERENCES

[1] J. Zander and P. Mähönen, "Riding the data tsunami in the cloud: Myths and challenges in future wireless access," *IEEE Commun. Mag.*, vol. 51, no. 3, pp. 145–151, Mar. 2013.
[2] Y. Song, P.-Y. Kong, and Y. Han, "Potential of network energy saving through handover in HetNets," *IEEE Trans. Veh. Technol.*, vol. 65, no. 12, pp. 10198–10204, Dec. 2016.
[3] K. Vasudeva, M. Simsek, D. López-Pérez, and İ. Güvenç, "Analysis of handover failures in heterogeneous networks with fading," *IEEE Trans. Veh. Technol.*, vol. 66, no. 7, pp. 6060–6074, Jul. 2017.
[4] B. Wang, Q. Kong, W. Liu, and L. T. Yang, "On efficient utilization of green energy in heterogeneous cellular networks," *IEEE Syst. J.*, vol. 11, no. 2, pp. 846–857, Jun. 2017.
[5] H. Saito and R. Kawahara, "Geometrical characterization of offloading through wireless LANs," *IEEE Trans. Mobile Comput.*, vol. 16, no. 1, pp. 130–142, Jan. 2017.
[6] M. Haenggi, J. G. Andrews, F. Baccelli, O. Dousse, and M. Franceschetti, "Stochastic geometry and random graphs for the analysis and design of wireless networks," *IEEE J. Sel. Areas Commun.*, vol. 27, no. 7, pp. 1029–1046, Sep. 2012.
[7] H. S. Dhillon, R. K. Ganti, F. Baccelli, and J. G. Andrews, "Modeling and analysis of K-tier downlink heterogeneous cellular networks," *IEEE J. Sel. Areas Commun.*, vol. 30, no. 3, pp. 550–560, Apr. 2012.
[8] H. S. Jo, Y. J. Sang, P. Xia, and J. G. Andrews, "Heterogeneous cellular networks with flexible cell association: A comprehensive downlink SINR analysis," *IEEE Trans. Wireless Commun.*, vol. 11, no. 10, pp. 3484–3495, Oct. 2012.
[9] H. Y. Kim, H. Kim, Y. H. Cho, and S.-H. Lee, "Self-organizing spectrum breathing and user association for load balancing in wireless networks," *IEEE Trans. Wireless Commun.*, vol. 15, no. 5, pp. 3409–3421, May 2016.
[10] N. Deng, W. Zhou, and M. Haenggi, "Heterogeneous cellular network models with dependence," *IEEE J. Sel. Areas Commun.*, vol. 33, no. 10, pp. 2167–2181, Oct. 2015.
[11] Y. J. Chun, M. O. Hasna, and A. Ghrayeb, "Modeling heterogeneous cellular networks interference using Poisson cluster processes," *IEEE J. Sel. Areas Commun.*, vol. 33, no. 10, pp. 2182–2195, Oct. 2015.
[12] Y. Xie, X. Zhang, Q. Cui, and Y. Lu, "User association for offloading in heterogeneous network based on matern cluster process," in *Proc. IEEE 85th Veh. Technol. Conf. (VTC Spring)*, Jun. 2017, pp. 1–5.
[13] M. Haenggi, *Stochastic Geometry for Wireless Networks*. New York, NY, USA: Cambridge Univ. Press, 2013.
[14] C.-H. Lee and Z.-S. Syu, "Handover analysis of macro-assisted small cell networks," in *Proc. IEEE Int. Conf. Internet Things (iThings), IEEE Green Comput. Commun.(GreenCom) IEEE Cyber, Phys. Soc. Comput. (CPSCom)*, Sep. 2014, pp. 604–609.
[15] S. N. Chiu, D. Stoyan, W. S. Kendall, and J. Mecke, *Stochastic Geometry and Its Applications*, 3rd ed. New York, NY, USA: Wiley, 2013.
[16] W. Bao and B. Liang, "Stochastic geometric analysis of user mobility in heterogeneous wireless networks," *IEEE J. Sel. Areas Commun.*, vol. 33, no. 10, pp. 2212–2225, Oct. 2015.
[17] W. Bao and B. Liang, "Handoff rate analysis in heterogeneous wireless networks with poisson and poisson cluster patterns," in *Proc. 16th ACM Int. Symp. Mobile Ad Hoc Netw. Comput.*, 2015, pp. 77–86.
[18] W. Bao and B. Liang, "Stochastic geometric analysis of handoffs in user-centric cooperative wireless networks," in *Proc. IEEE INFOCOM*, Apr. 2016, pp. 1–9.
[19] S. Sadr and R. S. Adve, "Handoff rate and coverage analysis in multi-tier heterogeneous networks," *IEEE Trans. Wireless Commun.*, vol. 14, no. 5, pp. 2626–2638, May 2015.
[20] S. Singh, H. S. Dhillon, and J. G. Andrews, "Offloading in heterogeneous networks: Modeling, analysis, and design insights," *IEEE Trans. Wireless Commun.*, vol. 12, no. 5, pp. 2484–2497, May 2013.
[21] X. Zhang, Y. Liu, Y. Wang, and J. Bai, "Performance analysis and optimization for nonuniformly deployed Mmwave cellular network," *EURASIP J. Wireless Commun. Netw.*, to be published.

XUEFEI ZHANG (M'15) received the B.E. and Ph.D. degrees in communications and information systems from the Beijing University of Posts and Telecommunications (BUPT), Beijing, China, in 2010 and 2015, respectively. She is currently a Lecturer with BUPT. Her current research interests mainly focus on networking technologies, vehicular network, big data, and mobile edge computing.

YUXUAN XIE received the B.S. degree in communication engineering from the University of Science and Technology of Beijing, Beijing, in 2015. She is currently pursuing the M.S. degree in communications and information systems with the Beijing University of Posts and Telecommunications. Her current research interests mainly focus on networking technologies.

YUSHAN CUI received the B.S. degree in communication engineering from Shandong University, Shandong, in 2016. She is currently pursuing the M.S. degree in communications and information systems with the Beijing University of Posts and Telecommunications. Her current research interests mainly focus on vehicular network and networking technologies.

QIMEI CUI (M'11) received the B.E. and M.S. degrees in electronic engineering from Hunan University, Changsha, China, in 2000 and 2003, respectively, and the Ph.D. degree in telecommunications from the Beijing University of Posts and Telecommunications (BUPT), Beijing, China, in 2006. She is currently a Professor with BUPT. Her current research interests mainly focus on transmission theories, networking technologies, green communications, and standardization for next-generation mobile communication networks.

XIAOFENG TAO (SM'13) received the B.S. degree in electrical engineering from Xi'an Jiaotong University, Xi'an, China, in 1993, and the M.S.E.E. and Ph.D. degrees in telecommunication engineering from the Beijing University of Posts and Telecommunications (BUPT), Beijing, China, in 1999 and 2002, respectively. He was the Chief Architect with the Chinese National FuTURE fourth-generation (4G) TDD Working Group from 2003 to 2006 and established the 4G TDD CoMP Trial Network in 2006. He is currently a Professor with BUPT. He is involved in the fifth-generation networking technology and mobile network security.